GSA DATA REPOSITORY 2013239 J.R. Gunnell et al.

Preface

In this appendix, we use ^{210}Pb-derived accretion rates to measure a landscape's elevation change. The proposed model assumes a constant rate of accretion and a constant initial concentration of radiotracer. It relies on the assumption that sediment grain size variation is minimal, that bioturbation does not occur, and that subsidence is negligible. We will validate these assumptions, explain our analysis, and explore its sensitivity.

Methods

The core at NM was taken from a boat with a 4" inner diameter polycarbonate tube attached to a push-coring apparatus. At sites B6, B7, B8, B10, B11, and B12, cores were taken by pounding 1.5 meter long, 4" diameter aluminum irrigation pipes into the marsh surface; compaction was not corrected for. These cores were extruded at one to two centimeter intervals and lyophilized for ^{210}Pb analysis. Cores for X-Ray images were taken using 50 by 10 by 3 cm plexiglass stab cores at sites B11 and MF. X-Ray exposures on these cores were collected with a digital X-Ray sensor. The MF stab core was dissected at one centimeter intervals and also was lyophilized for ^{210}Pb analysis.

Visible plant material was removed from the dry sediment with tweezers, and down-core ^{210}Pb variations were derived from selected 1.5 g sediment subsamples. These values were determined via isotope-dilution alpha spectrometry for the ^{210}Pb granddaughter isotope ^{210}Po, radioisotopes that are expected to be in secular equilibrium with each other (El-Daoushy et al., 1991). A ^{209}Po spike was added to each sample to determine chemical yield, then samples were microwave digested in stoppered teflon vessels with concentrated nitric acid. Hydrogen peroxide was added to the heated supernate from the digestion to extract the tracer from organic compounds (de Vleeschouwer et al., 2010), then the samples were brought to near dryness to remove nitric acid. In the next step, NH_4OH was added to the samples to induce iron scavenging. The precipitate was collected via centrifugation, dissolved with HCl, and prepared for plating onto stainless steel planchets with the addition of ascorbic acid to prevent oxides from interfering with spontaneous electrodeposition of Polonium (El-Daoushy et al., 1991). The activities of the Polonium tracers were determined via alpha spectrometry using silicon surface barrier detectors linked to a multichannel analyzer (Flynn, 1968).

Selected sediment samples were counted for gamma-emitting radiotracers in high purity germanium detectors. Detector efficiencies were verified using an IAEA standard. Samples were weighed into plastic petri dishes then sealed with parafilm. ^{40}K was measured using the 1460.1 keV photopeak, and ^{226}Ra was found by averaging the 295, 351.9, and 1120.2 keV photopeaks.

Core Description

Visual and X-Ray Analysis

Over the course of extrusion, each core was qualitatively described. Fibrous organic material deposited by marsh vegetation was most prevalent towards the surface of the cores, eventually vanishing down-core. This belowground biomass appeared to vary across cores as well, with a relatively low amount of fibrous organic material at the youngest sites (B11 and B12), and a greater amount at site B6, the oldest. Aside from variation in the predominance of plant matter, there were no other visually identifiable variations in samples over the course of extrusion. All sediments were cohesive gray muds.

The X-Rays (Figure D1) showed no evidence of bioturbation, with no visible burrowing animals or tubes. Pore spaces present in the B11 core were presumed to be from vegetation. This was corroborated by visual inspection during extrusion, where vegetative mass filled all apparent pore spaces, with no evidence of shells or tubes from bioturbators. There are visible surface laminations on the mudflat core, indicating unmixed sedimentation. Validating the visual inspection, the absence of especially bright laminations indicates that these cores are relatively homogenous with respect to material density, suggesting a lack of grain size variation. Nevertheless, there is a visible distinction between darker and lighter sequences halfway down the MF core, and this may indicate a subtle shift in porosity or mineralogy. Unfortunately, after transporting from the X-Ray facility, the core became partly desiccated before dissection for ^{210}Pb, making porosity measurements unreliable.

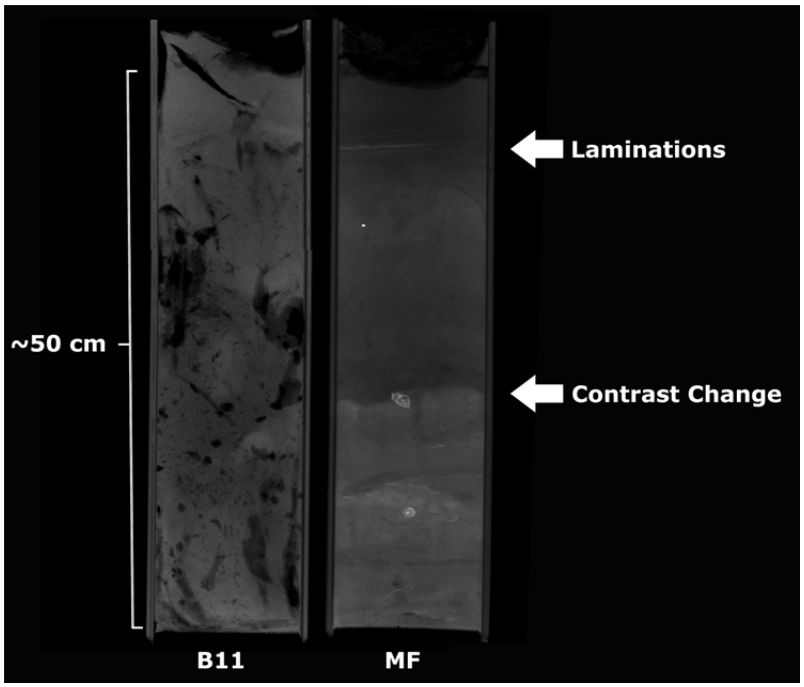

Figure DR1. X-Rays of stab cores. Note the pore-spaces in B11 at left; these were found to be associated with vegetation upon visual inspection. Major observations of MF are displayed at right.

Grain Size

Variation in grain size can alter the ^{210}Pb profile by changing the potential surface sorption sites for the radiotracer (Aalto and Nittrouer, 2012). However, such grain size variation has not been witnessed at the Newport field site. This portion of the river is the muddy bay-near stream section of the river. It is downstream of coarse mouth-bar deposits and upstream of the sandy tidal inlet, and is effectively protected from strong fluvial and tidal currents. As a result, it is muddy. A survey of sediment grab samples found that surface sediments in this portion of the river are predominantly clays and fine silts (Johnson, 1959). Surface sediments in a more recent study of the area corroborate this finding (Mattheus et al., 2010).

Historical findings and visual/X-ray analyses all suggest that these cores should have relatively homogenous, fine-grained lithologies. To validate this conclusion, we used the concentration of potassium (via ^{40}K) as a proxy for variation in lithology (Navas et al., 2002). Here, we assume that potassium is associated with the clay interlayer position, making its concentration proportional to the fine-grained sediment fraction of the sample. After deriving the geochronology (described later), the mudflat and marsh cores all displayed two sequences of sedimentation. There was a layer of rapidly accreting sediment overlying a layer of slowly accreting sediment. To ensure that this variation was not an artifact presented by a shift in lithology, the average ^{40}K concentration from selected samples in each sequence is compared (Fig. D2). Within each core, the concentrations found in each sequence are within error, and when all samples are combined the two sequences have nearly identical concentrations.

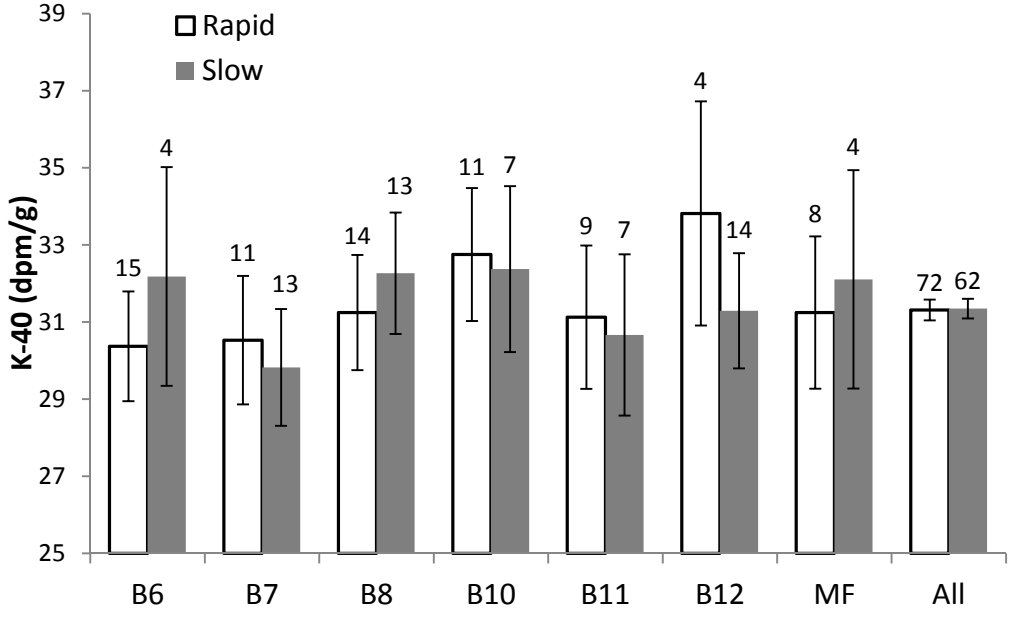

Figure DR2. Average ^{40}K Concentrations Comparisons. White bars represent samples taken from the rapidly accreting sequence of sediment, while gray bars represent samples taken from the slowly accreting sequence of sediment. The number of samples in each mean is displayed above individual error bars. Error bars are the root sum squares of the counting errors divided by the number of samples. Note truncated y-axis.

Analysis

Geochronology Choice and Implementation

Half-log projections of the excess ^{210}Pb profiles all exhibited a characteristic pattern of transitioning from one linear trend to another with higher slope (Fig. D3). In the right conditions, linear profiles are emblematic of a geochronology where the radiotracer has a constant initial concentration and the vertical accretion rate is constant (Appleby, 2001). This is often referred to as the "CIC model". In the following analysis, these break points are interpreted as a transition from one constant rate of accretion to another.

Mineralogical changes and bioturbation have been assessed and discounted in the core description section. Compaction will be addressed in a later section. The only conceivable remaining concern is that variation in the initial tracer concentration yielded these characteristic shifts in slope. In figure D4, we present different scenarios in some modeled ^{210}Pb profiles. As we can see in D4III and D4IV, there is a distinct discontinuity in the profile where the tracer concentration is doubled. A similar discontinuity would form if initial tracer concentrations were to change by a factor other than 2. In contrast, a comparison of Figure D3 and Figure D4II shows a similar profile where the two linear trends are connected end-on-end, transitioning into each other. Ultimately, these changes in slope are unlikely to result from a change in tracer concentration, otherwise there would be discontinuities in the profile.

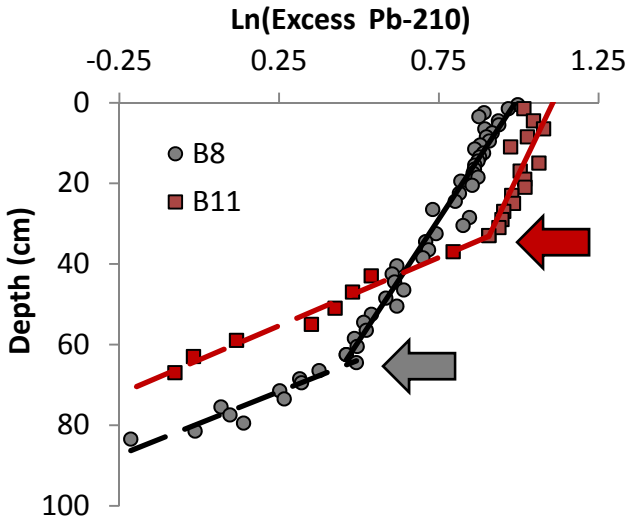

Figure DR3. Example plots of excess ^{210}Pb vs. Depth. Abrupt shifts in slope are indicated by arrows. Plots of each core are presented later in the appendix.

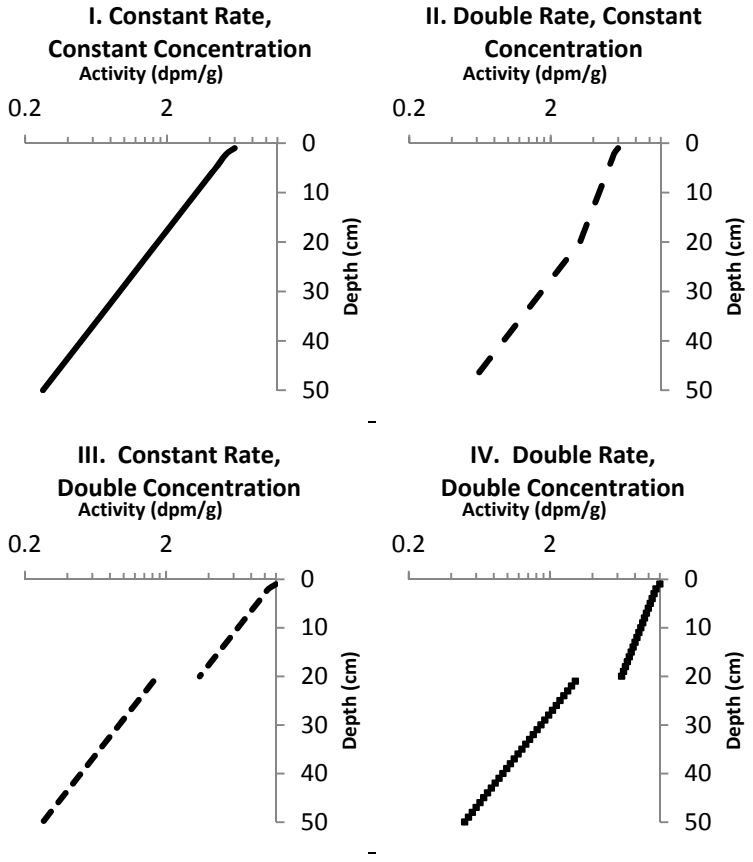

Figure DR4. Down-core Excess ^{210}Pb Scenarios. At 20 cm depth, II, III, and IV undergo a change in initial concentration and/or accretion rate.

Since the requisite assumptions are apparently satisfied, accretion rates were calculated along segments of the ^{210}Pb profiles using the CIC model. Linear regressions of excess ^{210}Pb vs. depth were made over intervals that provided the best r^2, the proportion of variability explained by the line (results in table 1). Each site had at least two linear intervals with distinctly different slopes, indicating a shift from one regime of constant accretion to another. Linear accretion rates progressed to the surface in all samples except NM, which had a mixed surface layer. One of the regressions was applied to a deeper section of NM below the mixed layer.

These linear intervals are well constrained by many data points, and regressions explained most of the variation in the data, indicating that a steady-state model of constant sediment accretion is appropriate. Derived sedimentation rates are proportional to the slope of the regression line (Equation D1). Error in the rate is proportional to standard error of the regression's slope. Due to the uncertainty in background ^{210}Pb, demonstrated in the standard deviation of the mean background values, accretion rates and their errors were calculated using regressions with three different background values (mean, mean+σ, mean-σ), with the final value being the root sum square of each result.

$$A = \frac{\lambda z}{\ln(\frac{C_0}{C_z})} = \lambda \times m \qquad \text{(Eq DR1)}$$

The rate of sediment accretion (A) is proportional to the depth interval (z) and the decay constant (λ), but inversely proportional to the natural logarithm of the change in tracer concentration (C) over that depth interval (Joshi and Shukla, 1991). This means that accretion rates are proportional to the slope (m) of a linear regression plotted through a depth profile of excess ^{210}Pb activities on the half-log scale.

Table DR. Results from elevation survey and linear regressions for accretion rates (elevation error is standard deviation of triplicate surveys)

Site	Elevation NAVD 88 (m)	(+/-)	Regression #	Depth Interval (cm)	n	Rate (cm/y)	(+/-)	r^2
B6	0.32	.012	1	0-59	39	0.97	0.04	0.98
			2	59-85	13	0.47	0.11	0.81
B7	0.46	.014	1	0-51	34	1.16	0.07	0.96
			2	51-77	13	0.23	0.06	0.80
B8	0.41	.015	1	0-63	41	1.61	0.10	0.95
			2	63-84	11	0.40	0.07	0.91
B10	0.31	.014	1	0-23	19	1.26	0.38	0.73
			2	23-53	15	0.65	0.07	0.95
			3	53-63	5	0.20	0.03	0.98
B11	0.26	.01	1	0-32	14	1.68	0.32	0.91
			2	32-68	8	0.46	0.04	0.98
B12	0.27	.016	1	0-24	9	1.16	0.18	0.93
			2	24-48	10	0.49	0.06	0.95
			3	48-64	4	0.23	0.04	0.98
MF	-0.28	.022	1	0-31	13	1.94	0.73	0.77
			2	31-53	11	0.33	0.12	0.70
NM	-0.55	.016	1	28-53	7	0.56	0.08	0.96
			2	53-63	9	0.20	0.05	0.86

Background ^{210}Pb Validation

Excess ^{210}Pb is the quantity of ^{210}Pb not supplied by in situ decay of its mother isotope, but rather by sorption of free ^{210}Pb from the water and atmosphere. Further addition of excess ^{210}Pb to sediment is prevented by burial. Over time, this excess signal decays and a background ^{210}Pb activity remains. Background ^{210}Pb is the product of in situ decay of Ra-226, which occurs continuously and results in secular equilibrium between the two isotopes. ^{210}Pb geochronologies are based on excess ^{210}Pb, but our sample preparation yields total ^{210}Pb. To find excess ^{210}Pb, the

background activity must be determined and subtracted from the total ^{210}Pb value (Appleby, 2001**)**. Three cores were deep enough to meet this background ^{210}Pb value: B6, B8, and NM. The background value for B6 was chosen to be the mean activity of samples 103-116 cm deep (.72 +/- .05 dpm/g). B8 was from 85-102.5 cm (1.1 +/- .07 dpm/g), and NM was from 74-126 (.67 +/- .06 dpm/g).

Other cores did not reach deep enough to provide estimates of background concentrations. Direct measurement of Ra-226 via gamma emission allows for comparison of background concentrations across cores (Fig. D5), demonstrating that the average background value is of comparable magnitude across cores. Unfortunately, these values can't be applied directly for calculations of excess ^{210}Pb. Our measurements of total ^{210}Pb are only of the acid-leachable fraction, whereas gamma-derived backgrounds measure both leachable sites and mineral lattices (Nittrouer et al., 1979). Regardless, it is apparent that background concentrations are quite similar throughout the sampling site, constraining potential estimates.

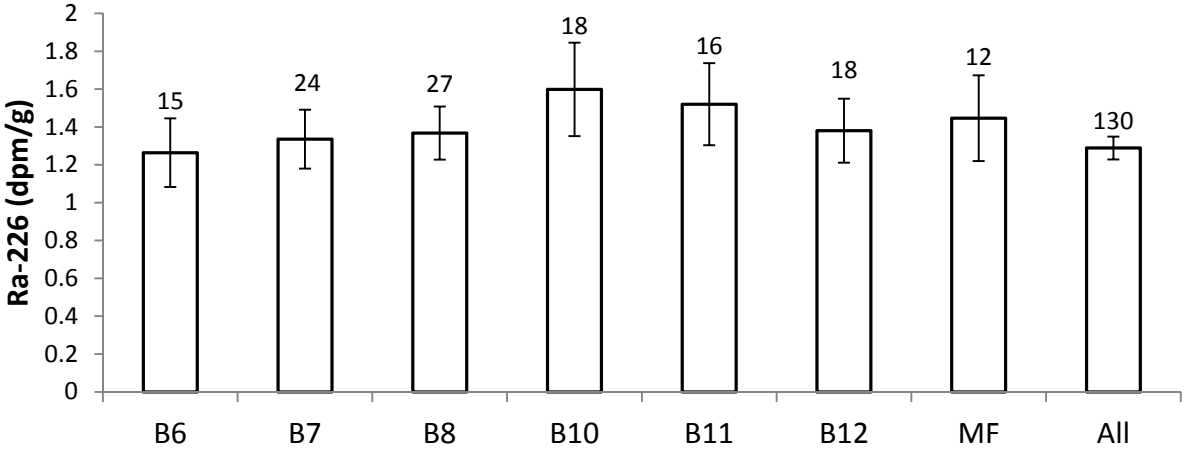

Figure DR5. Average Ra-226 by gamma detection. Error bars are the root sum squares of counting errors divided by the number of samples.

Final estimates of sediment accretion rates are potentially sensitive to error in the estimate of background-derived ^{210}Pb, because accretion rates are evaluated after excess ^{210}Pb estimates are log-transformed. When the background is changed from one value to another, the shift in the log-transformed estimate is described by Equation D2. As total ^{210}Pb values approach background, the resulting change in estimate, "D", is of greater magnitude (Fig. D6). If the initial estimate is high relative to the change in background, however, the change in estimate is close to zero. This means that estimates of more recent accretion patterns are less sensitive to variations in background. This effect manifests in our samples as we compare the relative change in estimated accretion rates against the average total ^{210}Pb of the data-points comprising the estimate (Fig. D7). Accretion rates derived from profiles with low excess ^{210}Pb concentrations were susceptible to changes in background estimates, whereas accretion rates with high concentrations were nearly unaffected.

$$D = Log(1 - \frac{\Delta}{I}) \qquad \text{(Eq DR2)}$$

Where "D" is the change in Log(excess ^{210}Pb), "Δ" is the change in background, and "I" is the initial estimate of excess ^{210}Pb.

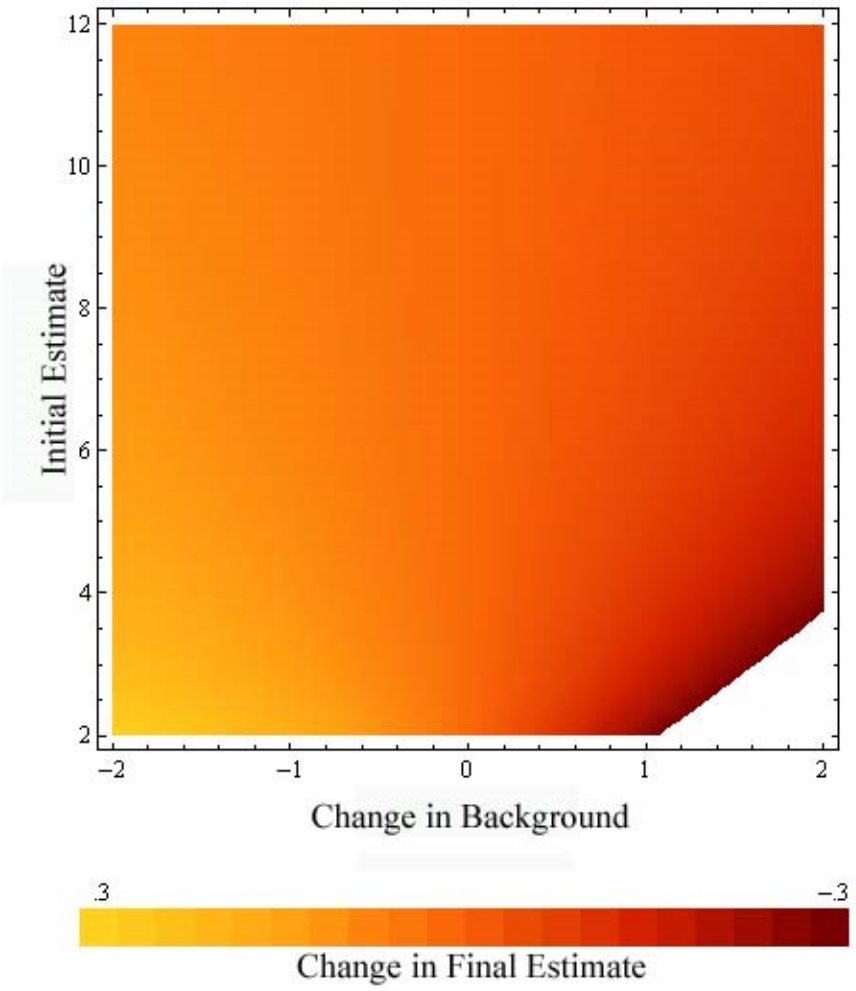

Figure DR6. Change in Log(Excess ^{210}Pb) when background is changed. Initial estimate and Change in background are in dpm/g. Changes in final estimate lower than -.3 are clipped.

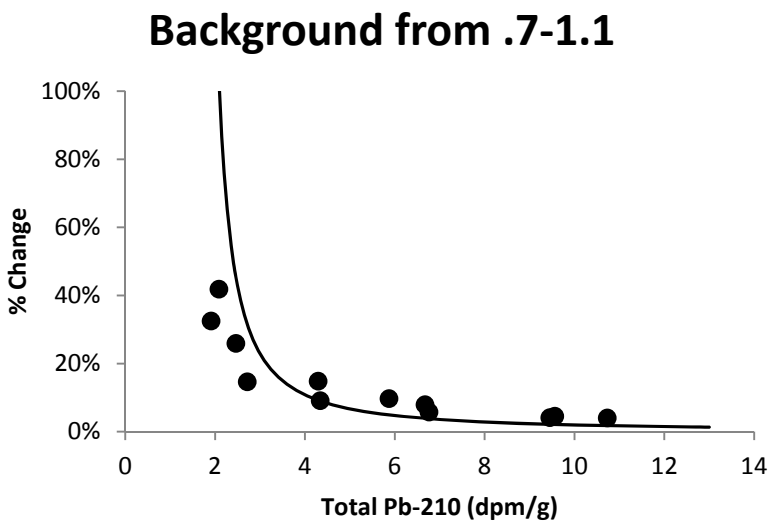

Figure DR7. Relative estimate change after changing background from .7 dpm/g to 1.1 dpm/g. The line is the relative change in dpm/g of an excess ^{210}Pb estimate after changing backgrounds. Using the terms from Eq. D2, the line is defined by D/Log(I). Data points are from accretion rates derived in this study and demonstrate the relative change in accretion rates after changing backgrounds.

Despite this apparent sensitivity to background estimates, variation in background does not alter the conclusions of this paper. According to the results section of the paper, sediment accretion rates are of sufficient precision to differentiate the date of the accretion break point from the date of marsh emergence. Since these events are in the more recent portion of the geochronology, they are less affected by changes in background estimate. Based on the ^{226}Ra measurements, it is expected that background values will be similar across marsh cores. Of the marsh cores that did not reach background, whether the background value from B6 (.67) or B8 (1.16) is used has no effect on the conclusion that the accretion break point happens before marsh emergence (Fig. D8). In both background scenarios, B7, B11, and B12 accelerated prior to marsh emergence, while it is unclear with B10. For consistency in the manuscript, all future assessments of excess ^{210}Pb in cores B7,B10,B11,B12, and MF use the background from B8.

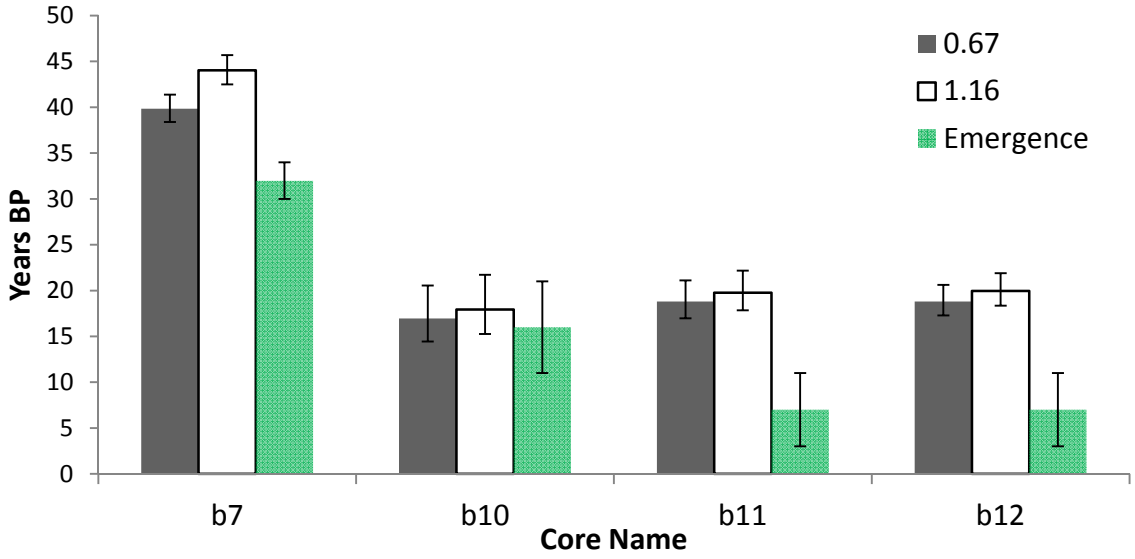

Figure DR8. Age comparison of breakpoints vs. marsh emergence using different background values [background value in legend (dpm/g)].

Compaction and Vertical Accretion Validation

The version of the CIC model utilized in this analysis looks at trends in the vertical distribution of the tracer profile. It's possible for this vertical distribution to be deformed by physical compaction or organic degradation, leading to an erroneous estimate for accretion rates (Mudd et al., 2009). Furthermore, compaction of underlying sediments can lead to shallow subsidence, decoupling sediment accretion rates from elevation change (Cahoon et al., 1995). Nevertheless, the ongoing emergence of marsh at this site indicates that accretion and elevation change must be coupled to some degree. Additionally, these radiometric assessments of vertical accretion match those found using other methods.

Using historical bathymetric maps, Wells 1996 found that the average vertical accretion in the open water of the Newport River Estuary was .5 cm/y. This matched estimates based on Cs-137 in the same study. Also using Cs-137, Williams 1998 found vertical accretion rates ranging from .15-.79 cm/y. All of these estimates are generally in agreement with rates found in the NM core and in the pre-breakpoint rates found in the marsh cores of this study. These independent investigations validate our analysis for bay-bottom accretion rates. The bathymetric estimate is especially meaningful because its agreement with the radiometric analyses indicates that subsidence is not appreciable in the open water. Additionally, if open water sediments are not significantly subsiding, then the bay-bottom sediments underlying the newly expanded marsh should not be subsiding either.

Similar to changes in bathymetry, changes in marsh elevation can also be used to find average rates of vertical accretion. Spartina Alterniflora begins to colonize near mean sea level, and mean sea level in the Morehead City, NC area is .118 m NAVD 88 (Hess et al., 2005). If the year of emergence (according to the aerial photography) is assumed to be at mean sea level, then the average accretion rate for the marsh is the change in elevation (from emergence to present)

divided by the number of years since emergence (Fig. D9). The change in elevation is found by taking the difference between surveyed elevations and the mean sea level elevation after correcting for local relative sea level rise (2.57+/-.44 mm/y) (Zervas 2009). The elevation-based rates are comparable to those from ^{210}Pb analysis and both methods yield rates that are faster than the .5 cm/y average accretion rate found on the bay-bottom. These independent corroborating estimates of bay-bottom and marsh accretion demonstrate that compaction probably is not a complicating factor at this site, and that ^{210}Pb geochronologies are effective tools for evaluating elevation change. Consequently, the rapid rates of marsh accretion relative to the bay bottom and the tight coupling of elevation change with ^{210}Pb-based accretion rates are both valid conclusions of our analyses.

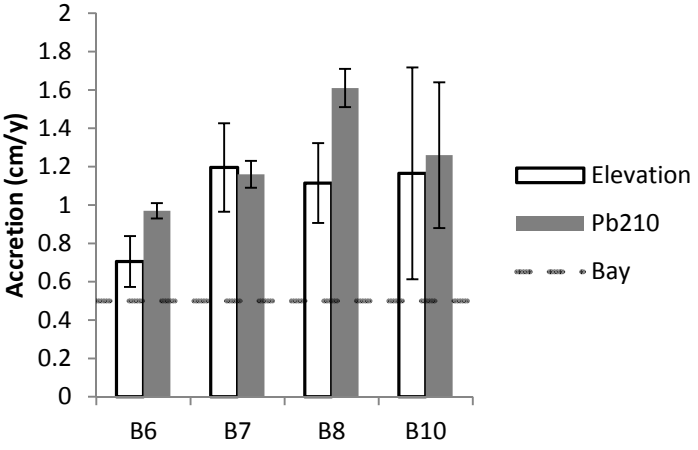

Figure DR9. Marsh Accretion Rates. "Elevation" indicates estimates made using the method described in the paragraph above. Its error bars are propagated from the years of emergence uncertainty found in the aerial photography and the confidence interval of the rate of sea level rise. "Bay" represents the .5 cm/y average accretion rate found in the bay bottom through multiple independent measures. Cores B11 and B12 were excluded from the comparison because the uncertainty of the year of emergence is too large relative to the number of years being estimated.

Conclusion

The analysis for vertical accretion of the bay and marsh was carried out using a CIC model of excess ^{210}Pb. We assessed the potential environmental complications prohibiting the implementation of this method, and addressed its sensitivity and error. After ruling out potential complications, we compared the results of our analysis to alternative measurements of vertical accretion at this site, ultimately validating our conclusions. Considering these factors, it is expected that this ^{210}Pb geochronology gives a reasonable longitudinal and temporal assessment of vertical accretion on this newly formed marsh.

Individual Plots:

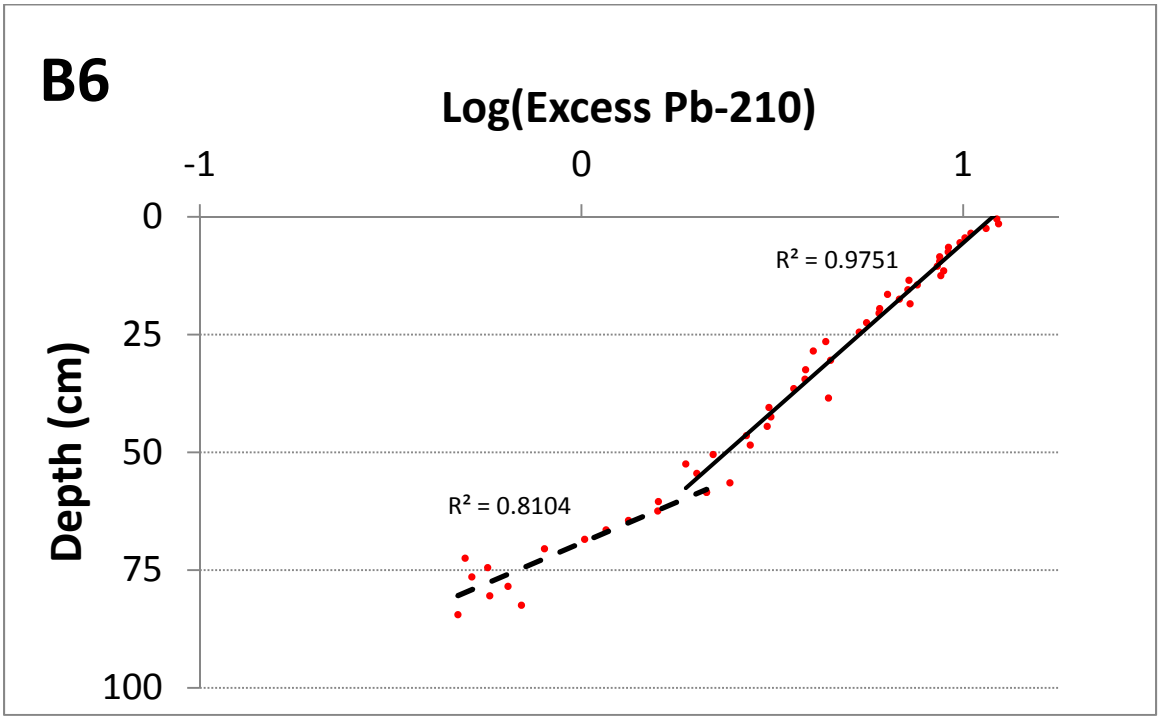

Figure DR10. Regressions of excess ^{210}Pb vs. depth at B6

Figure DR11. Regressions of excess ^{210}Pb vs. depth at B7

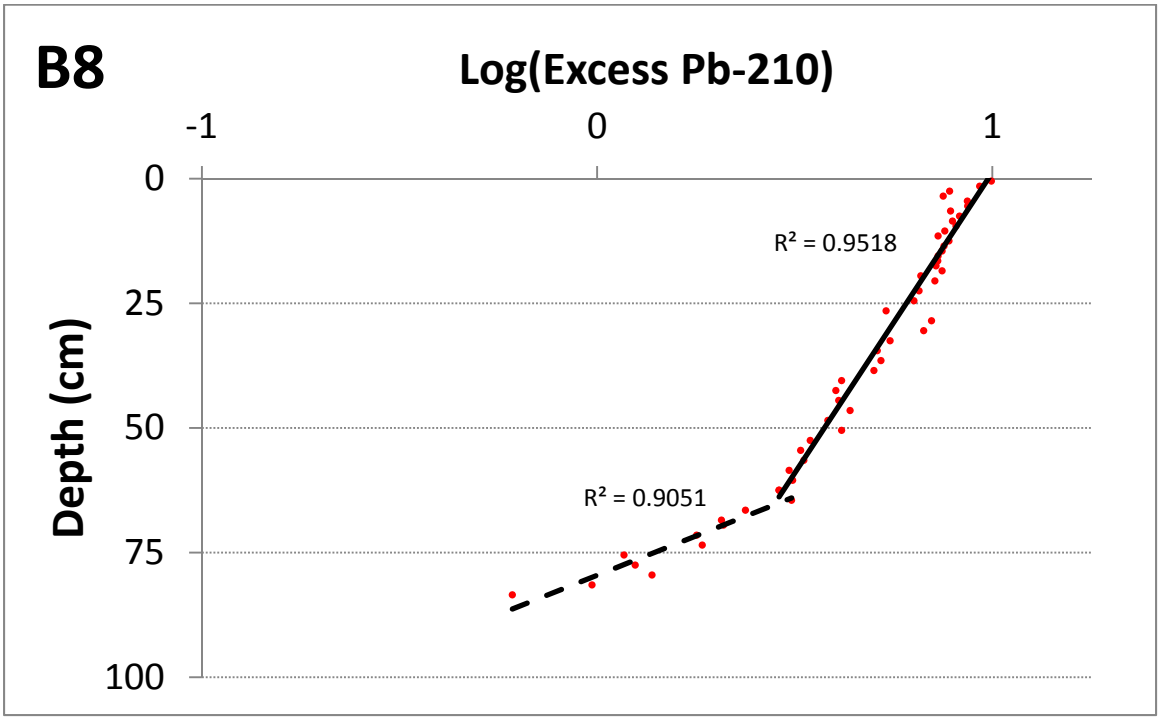

Figure DR12. Regressions of excess ^{210}Pb vs. depth at B8

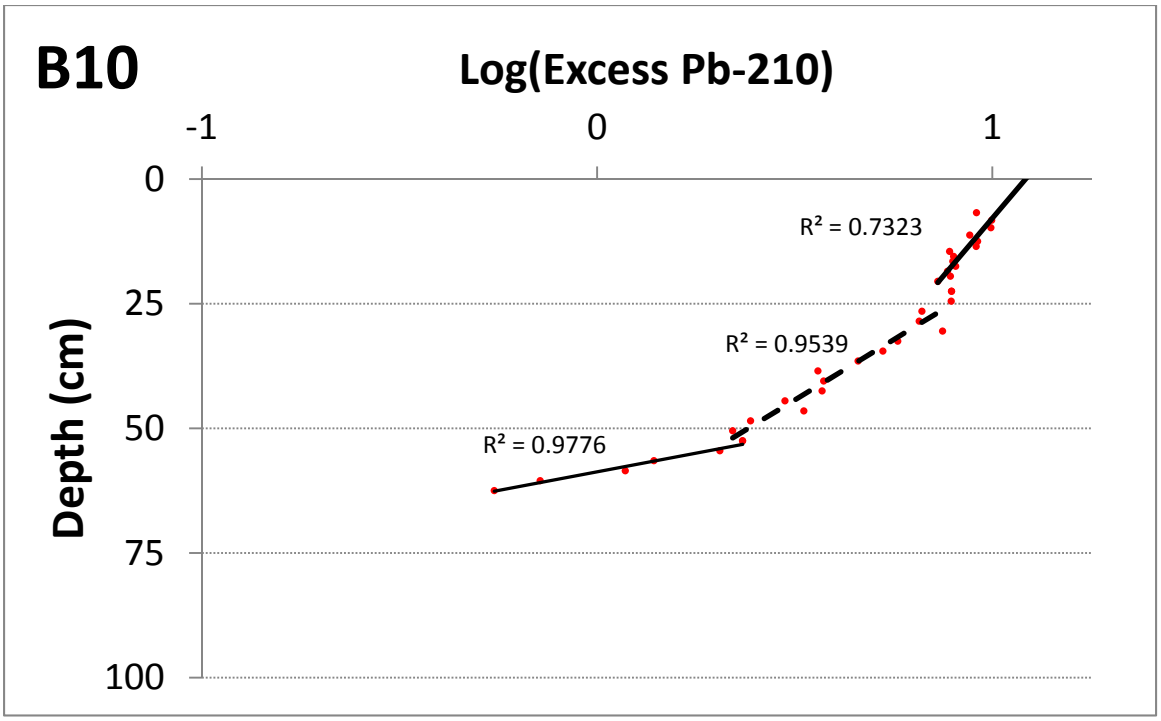

Figure DR13. Regressions of excess ^{210}Pb vs. depth at B10

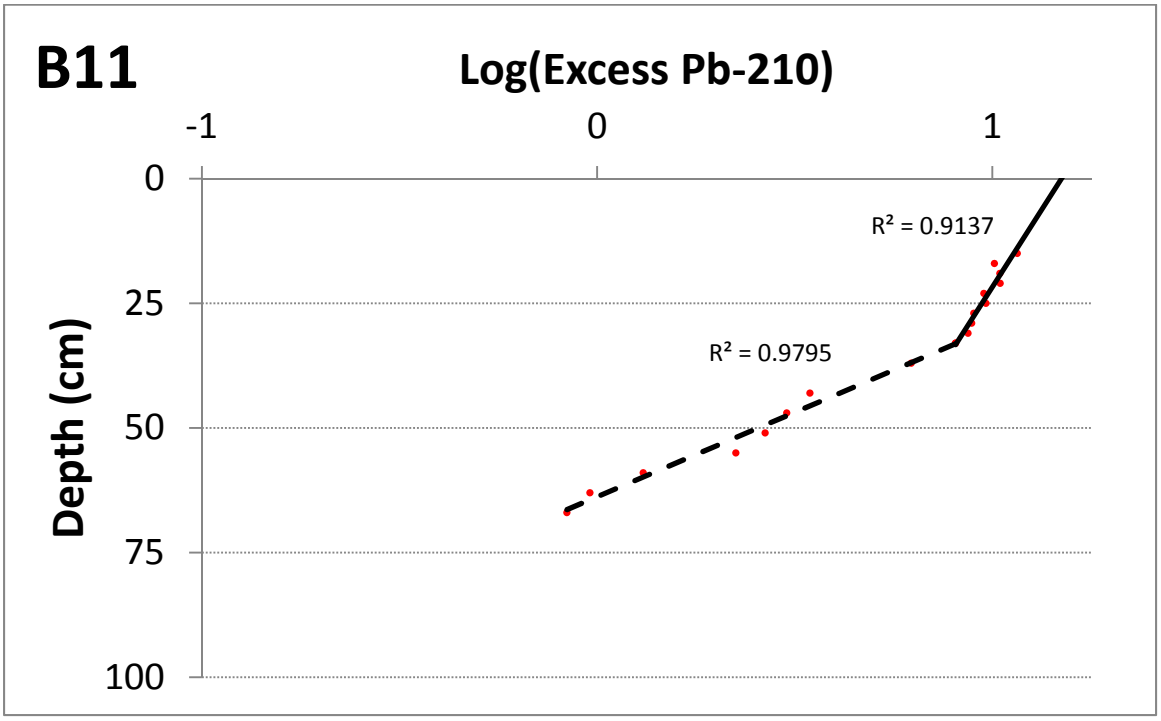

Figure DR14. Regressions of excess ^{210}Pb vs. depth at B11

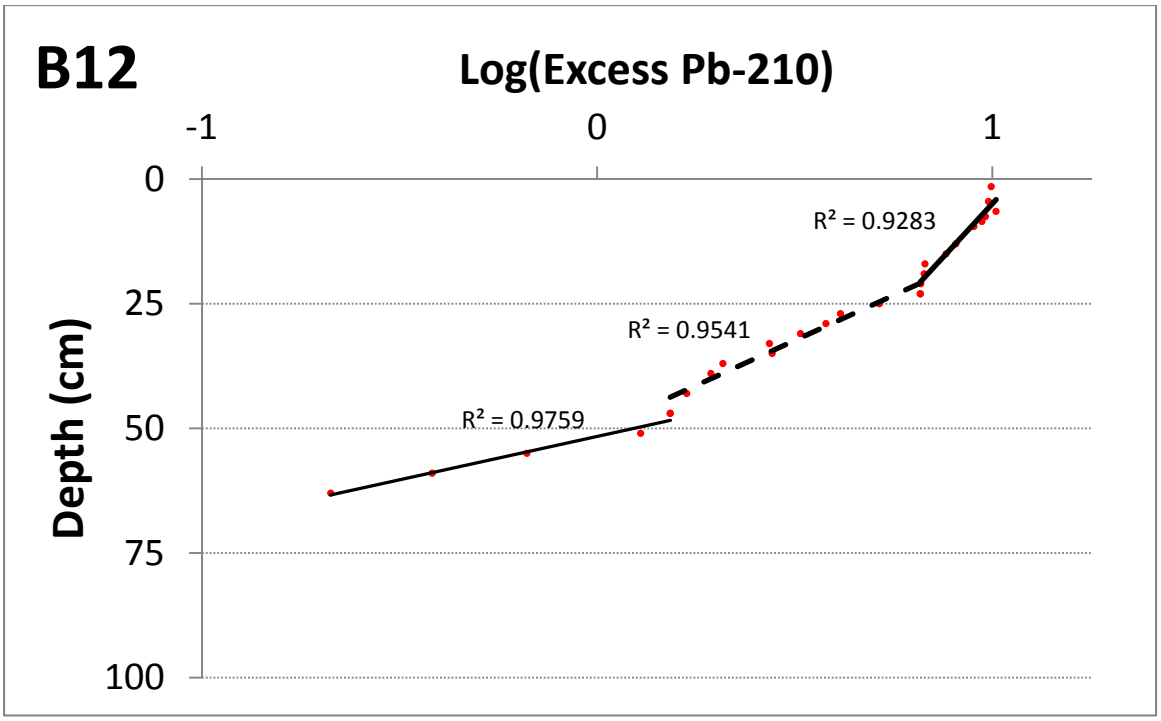

Figure DR15. Regressions of excess ^{210}Pb vs. depth at B12

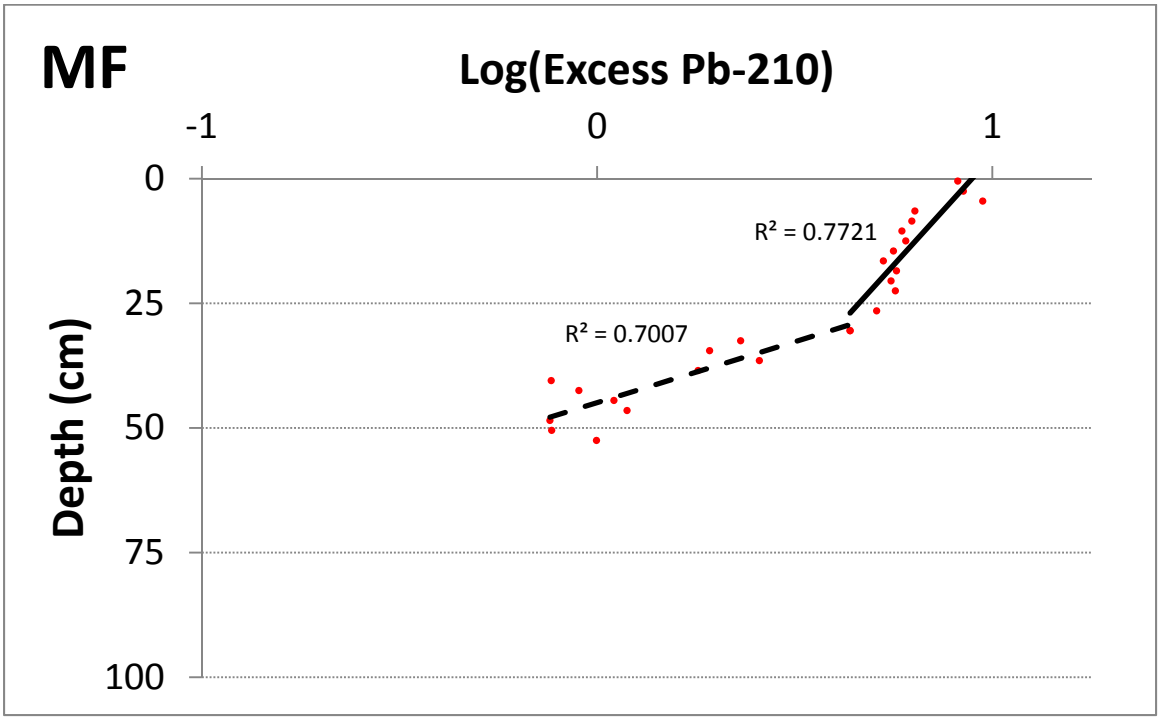

Figure DR16. Regressions of excess ^{210}Pb vs. depth at MF

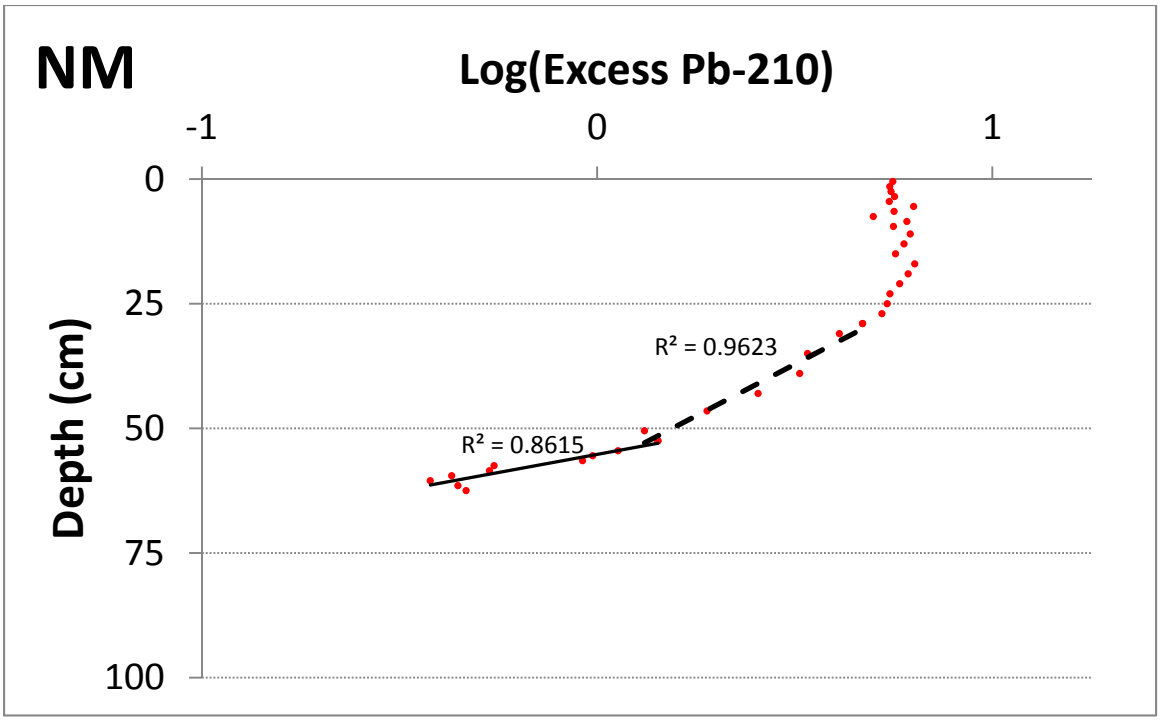

Figure DR17. Regressions of excess ^{210}Pb vs. depth at NM

References

Aalto, R., and Nittrouer, C.A., 2012, 210Pb geochronology of flood events in large tropical river systems: Philosophical Transactions of the Royal Society: Mathematical, Physical and Engineering Sciences, v. 370, no1966, p. 2040-2074.

Appleby, P.G., 2001, Chronostratigraphic Techniques in Recent Sediments, *in* Last, W.M. and Smol, J.P. eds., Tracking Environmental Change Using Lake Sediments. Volume 1: Basin Analysis, Coring, and Chronological Techniques, Kluwer Academic Publishers, Dordercht, The Netherlands, p. 171-203.

Cahoon, D., 1995, Estimating shallow subsidence in microtidal salt marshes of the southeastern United States: Kaye and Barghoorn revisited: Marine Geology, v. 128, no. 1-2, p. 1-9, doi: 10.1016/0025-3227(95)00087-F.

El-Daoushy, F., Olsson, K., and Garcia-Tenorio, R., 1991, Accuracies in Po-210 determination for lead-210 dating: Hydrobiologia, v. 214, no. 1, p. 43–52, doi: 10.1007/BF00050930.

Flynn, W., 1968, The determination of low levels of polonium-210 in environmental materials: Analytica chimica acta, v. 43, p. 221–227.

Hess, K.W., Spargo, E.A., Wong, A., White, S.A., Gill, S.K., 2005, VDATUM for Central Coastal North Carolina: Tidal Datums, Marine Grids, and Sea Surface Topography: National Oceanic and Atmospheric Administration Open-File Report NOS-CS-21.

Johnson, F.K., 1959, The Sediments of the Newport River Estuary, Morehead City, North Carolina [Master's Thesis]: Chapel Hill, University of North Carolina, 36p.

Joshi, S., and Shukla, B., 1991, Ab initio derivation of formulations for 210 Pb dating of sediments: Journal of Radioanalytical and Nuclear Chemistry, v. 148, no. 1, p. 73–79.

Mattheus, C.R., Rodriguez, A.B., McKee, B.A., Currin, C.A., 2010, Impact of land-use change and hard structures on the evolution of fringing marsh shorelines: Estuarine, Coastal and Shelf Science, v. 88, no 3, p. 365-376.

Mudd, S.M., Howell, S.M., and Morris, J.T., 2009, Impact of dynamic feedbacks between sedimentation, sea-level rise, and biomass production on near-surface marsh stratigraphy and carbon accumulation: Estuarine, Coastal and Shelf Science, v. 82, no. 3, p. 377-389, doi: 10.1016/j.ecss.2009.01.028.

Navas, A., Soto, J., and Machin J., 2002, 238U, 226Ra, 210Pb, 232Th and 40K activities in soil profiles of the Flysch sector(Central Spanish Pyrenees): Applied Radiation and Isotopes, v. 57, p. 579–589

Nittrouer, C. A., Sternberg, R.W., Carpenter, R., Bennett, J.T., 1979, The use of Pb-210 geochronology as a sedimentological tool: application to the Washington continental shelf: Marine Geology, v. 31, no 3, p. 297-316.

de Vleeschouwer, F., Sikorski, J., and Fagel, N., 2010, Development of Lead-210 Measurement in Peat Using Polonium Extraction. A Procedural Comparison: Geochronometria, v. 36, no. -1, p. 1-8, doi: 10.2478/v10003-010-0013-5.

Wells, J.T., 1996, Newport River Estuary Siltation Study: Report to Fishery Resource Grant Program. Contract No. M6007.

Williams, A.A., 1998, Sediment accumulation rates in the Newport River estuary: a 137Cs and 210Pb approach [Master's Thesis]: Chapel Hill, University of North Carolina, 75 p.

Zervas, C, 2009, Sea Level Variations of the United States 1854-2006: National Oceanic and Atmospheric Adminstration Open-File Report NOS CO-OPS 053.